Eocene atmospheric CO_2 from the nahcolite proxy

Elliot A. Jagniecki*, Tim K. Lowenstein, David M. Jenkins, and Robert V. Demicco
Department of Geological Sciences and Environmental Studies, Binghamton University, Binghamton, New York 13902, USA

ABSTRACT

Estimates of the atmospheric concentration of CO_2, $[CO_2]_{atm}$, for the "hothouse" climate of the early Eocene climatic optimum (EECO) vary for different proxies. Extensive beds of the mineral nahcolite ($NaHCO_3$) in evaporite deposits of the Green River Formation, Piceance Creek Basin, Colorado, USA, previously established $[CO_2]_{atm}$ for the EECO to be >1125 ppm by volume (ppm). Here, we present experimental data that revise the sodium carbonate mineral equilibria as a function of $[CO_2]$ and temperature. Co-precipitation of nahcolite and halite (NaCl) now establishes a well-constrained lower $[CO_2]_{atm}$ limit of 680 ppm for the EECO. Paleotemperature estimates from leaf fossils and fluid inclusions in halite suggest an upper limit for $[CO_2]_{atm}$ in the EECO from the nahcolite proxy of ~1260 ppm. These data support a causal connection between elevated $[CO_2]_{atm}$ and early Eocene global warmth, but at significantly lower $[CO_2]_{atm}$ than previously thought, which suggests that ancient climates on Earth may have been more sensitive to a doubling of $[CO_2]_{atm}$ than is currently assumed.

INTRODUCTION

The Eocene was the longest warm climate period of the Cenozoic, peaking during the early Eocene climatic optimum (EECO) at ca. 52–50 Ma and ending with the development of Antarctic ice sheets at ca. 34 Ma (Zachos et al., 2008). New estimates of the atmospheric concentration of CO_2, $[CO_2]_{atm}$, from alkenones in phytoplankton from Ocean Drilling Program (ODP) Site 925 give concentrations of ~700–1200 ppm by volume (ppm hereafter) from the middle–late Eocene to the early Oligocene (ca. 39–28 Ma), dropping to <500 ppm by the end of the Oligocene (ca. 23 Ma) (Zhang et al., 2013). These results suggest a connection between decreasing $[CO_2]_{atm}$, global cooling, and the development of Antarctic ice sheets. Establishing a causal relationship between $[CO_2]_{atm}$ and the "hothouse" climate of the EECO, however, has been more difficult because proxies show a wide range of estimated $[CO_2]_{atm}$, from pre-industrial values of 280 ppm to ~1870 ppm (Fig. 1; Royer, 2014). Here, we present new mineral equilibrium data that revise the nahcolite proxy and change the $[CO_2]_{atm}$ lower limit for the EECO to 680 ppm. This provides a firm physicochemical constraint that is independent of other $[CO_2]_{atm}$ proxies that have suggested significantly higher (and lower) values, such as paleosols and leaf stomata (see below). The new nahcolite proxy, when used in conjunction with paleotemperature estimates from fossil leaf-margin analysis and homogenization temperatures of fluid inclusions in halite, suggests an upper limit of ~1260 ppm for $[CO_2]_{atm}$ during the EECO. These results show that $[CO_2]_{atm}$ may not have been as high as previously thought during the warmest interval of the Cenozoic, implying a climate sensitivity for CO_2 that is roughly twice as high as is currently assumed (Royer et al., 2012).

Early Eocene $[CO_2]_{atm}$ Proxies

For the early Eocene (ca. 56–49 Ma), $[CO_2]_{atm}$ has been estimated from (1) paleosols (Cerling, 1992; Sinha and Stott, 1994; Ekart et al., 1999; Royer et al., 2001; Yapp, 2004; Breecker et al., 2010; Hyland and Sheldon, 2013; Hyland et al., 2013); (2) leaf stomata (McElwain, 1998; Retallack, 2001; Royer, 2003; Greenwood et al., 2003; Beerling et al., 2009; Smith et al., 2010; Franks et al., 2014); (3) a liverwort (bryophyte)

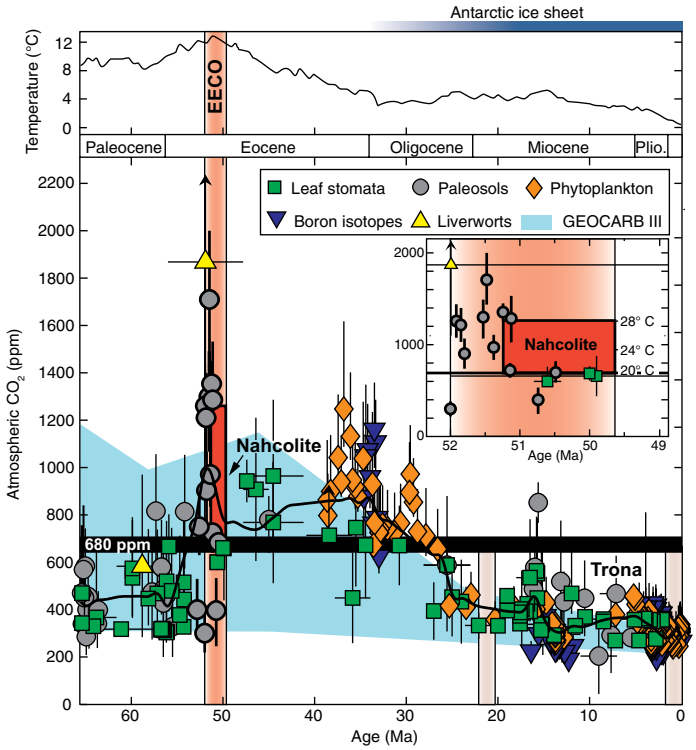

Figure 1. Atmospheric concentration of CO_2, $[CO_2]_{atm}$, over the past 65 m.y. reconstructed from terrestrial and marine proxies (see Data Repository [see footnote 1] for references) following recent revisions (Royer, 2014). Upper panel shows global deep-sea temperatures calculated from $\delta^{18}O$ record (Zachos et al., 2008) after protocol of Hansen et al. (2008). Inception of Antarctic ice sheets (ca. 34 Ma) (blue bar) (Zachos et al., 2008) coincides with deep-sea temperatures of <~4 °C and $[CO_2]_{atm}$ < ~600 ppm (lower panel). Pink vertical bar corresponds to maximum deep-sea temperature (~12 °C) during the early Eocene climatic optimum (EECO) and deposition of nahcolite in the Green River Formation (Colorado, USA). Lines on proxy symbols show reported uncertainties. Paleosol $[CO_2]_{atm}$ in bold (Hyland and Sheldon, 2013; Hyland et al., 2013) is estimated after methods of Cotton and Sheldon (2012) for calculating soil respired CO_2. Black horizontal line shows minimum pCO_2 (680 ppm) necessary to precipitate nahcolite. Red rectangle for Green River nahcolite (51.3–49.6 Ma) shows probable range of 680–1260 ppm $[CO_2]_{atm}$ for nahcolite precipitation. Light pink bars indicate lower $[CO_2]_{atm}$ for deposition of trona from Beypazari, Turkey (21.5 ± 0.9 Ma) and Searles Lake, California,USA (<1 Ma) (Lowenstein and Demicco, 2006). Black line is 15-point running average through each million-year data point. GEOCARB III $[CO_2]_{atm}$ is calculated from modeling the carbon cycle over long time scales and the exchange of carbon between the atmosphere and rocks (Berner and Kothavala, 2001). Inset shows details for 52–49 Ma and estimated $[CO_2]_{atm}$ from nahcolite, paleosols (Hyland and Sheldon, 2013; Hyland et al., 2013), leaf stomata (Greenwood et al., 2003; Smith et al., 2010; Franks et al., 2014), and liverworts (Fletcher et al., 2008). Plio.—Pliocene.

*Current address: ConocoPhillips Company, 600 North Dairy Ashford, Houston, Texas 77079, USA.

fossil (Fletcher et al., 2008); (4) marine boron isotopes (Pearson and Palmer, 2000); and (5) the sodium carbonate mineral nahcolite (Lowenstein and Demicco, 2006) (Fig. 1; see the GSA Data Repository[1] for a complete list of references used for Fig. 1). All of these estimates, except that from nahcolite, are indirect proxy measurements that depend on various calibrations to arrive at a $[CO_2]_{atm}$, and all have been subject to criticism (Royer, 2014). Some proxies, for example paleosols (Hyland and Sheldon, 2013; Hyland et al., 2013) and leaf stomata (Greenwood et al., 2003; Smith et al., 2010; Franks et al., 2014), have been updated and have lowered $[CO_2]_{atm}$ estimates for the early Eocene, changing the previous upper boundary from ~3500 ppm to ~1800 ppm (Fig. 1). But the range of $[CO_2]_{atm}$ is still large due to discrepancies between proxy methods, individual proxy errors, and temporal variability.

REFINEMENT OF THE NAHCOLITE PROXY

The equilibrium assemblage of the evaporite minerals nahcolite ($NaHCO_3$) and trona ($NaHCO_3{\cdot}Na_2CO_3{\cdot}2H_2O$) in the Green River Formation, Piceance Creek Basin, Colorado, USA (51.3–48.9 Ma) (Smith and Carroll, 2015) previously established a lower $[CO_2]_{atm}$ limit of 1125 ppm for the EECO (Lowenstein and Demicco, 2006) (Fig. 2; Fig. DR1 in the Data Repository). Earlier experiments demonstrated that in the Na_2CO_3-$NaHCO_3$-CO_2-H_2O system, nahcolite precipitates at higher $[CO_2]$ levels, >1330 ppm, and >1125 ppm in a halite-saturated brine (Eugster, 1966) (Fig. 3). Trona may form at the same $[CO_2]$ as nahcolite but only at higher temperatures; natron ($Na_2CO_3{\cdot}10H_2O$) forms at low $[CO_2]$ and low temperatures. New equilibrium experiments described here better define the nahcolite-trona-natron triple point and show that nahcolite precipitates at substantially lower $[CO_2]$ values than was reported by Eugster (1966).

Experimental Materials, Methods, and Results

The minimum $[CO_2]$ at which nahcolite is stable occurs at the triple point where nahcolite, trona, and natron are all at equilibrium (Fig. 3). We investigated three reversible reactions under controlled temperatures and known $[CO_2]$ because together they define the triple point and thus constrain the minimum $[CO_2]$ for the EECO:

$$3NaHCO_3\,(\text{nahcolite}) + H_2O_{(l)} = Na_2CO_3{\cdot}NaHCO_3{\cdot}2H_2O\,(\text{trona}) + CO_{2(g)}, \quad (1)$$

$$2NaHCO_3\,(\text{nahcolite}) + 9H_2O_{(l)} = Na_2CO_3{\cdot}10H_2O\,(\text{natron}) + CO_{2(g)}, \quad (2)$$

and

$$2Na_2CO_3{\cdot}NaHCO_3{\cdot}2H_2O\,(\text{trona}) + 25H_2O_{(l)} = 3Na_2CO_3{\cdot}10H_2O\,(\text{natron}) + CO_{2(g)}, \quad (3)$$

where l is liquid, g is gas, and quantities of reactants and products are stoichiometric proportions.

Mineral equilibria were investigated by mixing stoichiometric proportions of synthetic mineral phases with the appropriate weight percent of H_2O given in Reactions 1–3 (for details, see the Data Repository). Growth and breakdown of nahcolite, trona, and natron were quantified by X-ray diffraction (XRD), where peak-area ratios of the phases were compared to the original starting reaction mixture (Tables DR1–DR3 in the Data Repository; Fig. DR3). XRD analysis bracketed univariant boundaries at known temperatures (±0.1 °C) and $[CO_2]$ (±2% ppm). Standard enthalpy of formation ($\Delta H^\circ_{f,298}$) and standard third-law entropy (S°_{298}) for trona and natron were derived from the experimental results and calibrated to the extant thermodynamic data for nahcolite, $H_2O_{(l)}$, and $CO_{2(g)}$ (for details, see the Data Repository; Fig. DR4). Phase boundaries for Reactions 1–3 were then calculated in $[CO_2]$-temperature space using the derived enthalpies and entropies. The experimental results produce a downward revision of the nahcolite-trona-natron triple point to 840 ppm (19.5 °C), and 680 ppm for the nahcolite-trona univariant boundary at halite saturation (19.5 °C) (Fig. 3; Fig. DR5), and thus establish a new, lower $[CO_2]_{atm}$ limit for the EECO (Fig. 1).

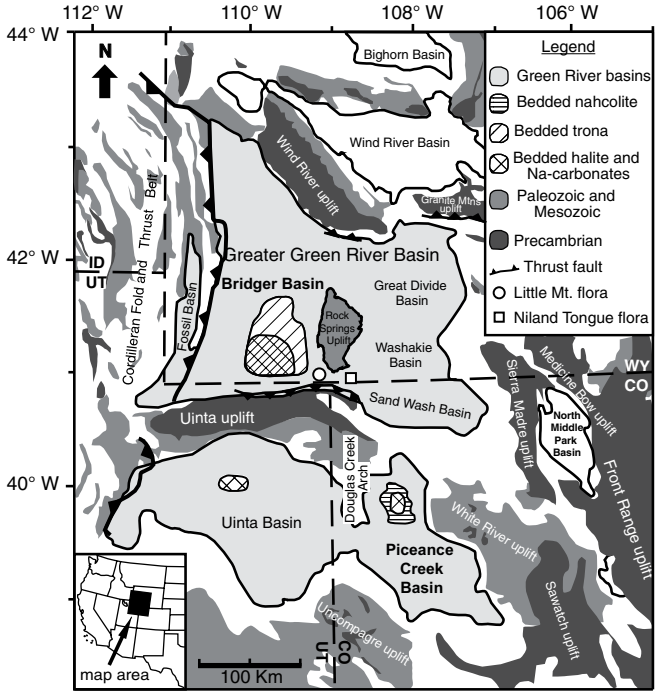

Figure 2. General geologic map of Green River Formation basins and extent of saline mineral deposits. Nahcolite deposits occur in the Piceance Creek Basin (Colorado, USA) and trona deposits in the Bridger Basin (Wyoming). Location of fossil leaf assemblages (circle and square) are from Wilf (2000). Modified from Smith and Carroll (2015) and Dyni (1996).

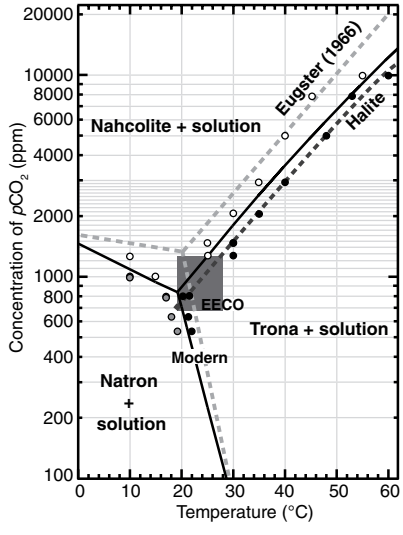

Figure 3. Stability fields of nahcolite, trona, and natron constructed from Reactions 1–3 (see text) as function of $[CO_2]$ and temperature. Minerals and solution are in equilibrium with gas at 1 atm total pressure. Circles are experimental data points that bracket mineral stability boundaries (solid black lines); white circles are nahcolite stable, black circles are trona stable, and gray circles are natron stable. Phase boundaries were calculated from derived thermochemical data (see Data Repository [see footnote 1]). Lower limit of nahcolite stability is $[CO_2]$ of 840 ppm at 19.5 °C (triple point) and $[CO_2]$ of 680 ppm with NaCl added to the system (19.5 °C). Dark gray box shows sodium carbonate precipitation in early Eocene ($[CO_2]_{atm}$ ~680–1260 ppm) over temperature range of 19.5–28.0 °C, compared to modern ($[CO_2]_{atm}$ = 400 ppm). Dashed light gray line from previous work of Eugster (1966). EECO—early Eocene climatic optimum.

[1]GSA Data Repository item 2015357, compiled references and supporting text for Figure1, geologic cross sections (Fig. DR1), thin-section of nahcolite (Fig. DR2), experimental methods for Reactions 1–3, derivation of thermochemical calculations, Tables DR1–DR4, and Figures DR3–DR5, is available online at www.geosociety.org/pubs/ft2015.htm, or on request from editing@geosociety.org or Documents Secretary, GSA, P.O. Box 9140, Boulder, CO 80301, USA.

Nahcolite Deposition

More than 32×10^9 metric tons of nahcolite have been found in the Green River Formation (Dyni, 1996) (Fig. 2). It occurs at basin center within the Parachute Creek Member as bedded deposits in strata up to 340 m thick, and with an aerial extent of ~680 km^2 (Dyni, 1996). The strata are of similar age (51.3–48.9 Ma) and origin (evaporative saline lake) to the laterally extensive trona-bearing strata of the Wilkins Peak Member, Bridger Basin, Wyoming, ~200 km to the northwest (Smith and Carroll, 2015) (Fig. 2; Fig. DR1).

The nahcolite is interbedded with organic-rich carbonate mudstone and, in places, is finely interlayered with halite (Dyni, 1996; Lowenstein and Demicco, 2006). Nahcolite laminae are composed of detrital microcrystalline chemical "mud" (prisms ~10 µm and up to 150 µm in length) and halite cumulates consisting of small cubes (millimeter to sub-millimeter size) and larger halite rafts (up to 7 mm in length) (Fig. DR2). We infer that nahcolite and halite crystals precipitated in the water column and settled down to the brine bottom where they formed layered deposits. Commonly, crystals of nahcolite and halite form drapes on top of bottom-growth halite crusts that thicken between halite crystals and thin at their tops, as would be expected of deposits that settled from suspension (Fig. DR2). Relatively large halite crystal rafts probably formed at the air-water interface, held there by surface tension (Lowenstein and Hardie, 1985). Such surface tension–controlled features suggest that co-precipitation of halite and nahcolite occurred at the air-water interface of a hypersaline lake, in contact with the atmosphere, and are therefore a direct consequence of the $[CO_2]_{atm}$ at the time (Lowenstein and Demicco, 2006).

Bottom-growth halite crusts contain clear crystals indicating slow precipitation into an open, halite-saturated brine body (Fig. DR2). By comparison, halite that crystallizes rapidly in shallow (<1 m) brine pools typically is clouded with dense fluid inclusion–rich bands (Lowenstein and Hardie, 1985). The absence of any sedimentary dissolution features in bedded nahcolite-halite from the Piceance Creek Basin suggests that deposition occurred in a perennial, stratified hypersaline lake in which deposits were protected from undersaturated surface waters by denser bottom brines. In contrast, evaporites formed in shallow non-stratified systems are typically "recycled" by dilute floodwaters that leave a distinctive record of partial to complete dissolution of the crystalline framework.

Paleotemperature Constraints on EECO $[CO_2]_{atm}$

Knowledge of the lake water temperatures at which nahcolite precipitated in the EECO is important for further constraining $[CO_2]_{atm}$. This is because the $[CO_2]$ at which nahcolite precipitates rises substantially as temperature rises, from a lower limit of 680 ppm at 19.5 °C to 1910 ppm at 34 °C (referenced to a halite-saturated system) (Fig. 3). Paleotemperature estimates from fossil leaf-margin analysis indicate subtropical climates in the Greater Green River Basin, with mean annual temperatures (MATs) of 23.0 °C just before, and 19.6 °C after, nahcolite deposition (Wilf, 2000). The leaf fossils occur at the basin margin in mixed lacustrine-alluvial deposits near the Uinta Mountain front (Fig. 2); some of these plant materials could have been transported from the highlands to the site of deposition (Wilf, 2000). The above MATs may therefore reflect conditions near the Uinta Mountains, not the lower-elevation basin center where temperatures were likely higher, especially during summer months.

Homogenization temperatures measured from primary fluid inclusions in cumulate halite in the Green River Formation, Piceance Creek Basin, give more relevant information on the temperatures of nahcolite precipitation. Fluid inclusion homogenization temperatures range from 21 to 28 °C (weighted average, with mean = 24.5 °C), indicating diurnal and seasonal surface water temperature variations (LaClair and Lowenstein, 2010). By comparison, the modern Dead Sea surface-water temperatures vary seasonally from ~21 to 36 °C (Neev and Emery, 1967). The Dead Sea is a robust analog for the Eocene Piceance Creek Basin lakes because it is at halite saturation and has a similar surface area–to–water depth ratio (Neev and Emery, 1967; Johnson, 1981). Considering the above fluid-inclusion temperatures and the Dead Sea analog, average surface-water temperatures of 21–28 °C during precipitation of nahcolite and halite in the Piceance Creek Basin are reasonable, which corresponds to $[CO_2]_{atm}$ values of ~760–1260 ppm for the EECO (Figs. 1 and 3).

The nahcolite-trona univariant boundary at halite saturation, 19.5 °C (680 ppm), is a robust constraint on the lower $[CO_2]_{atm}$ limit in the EECO; $[CO_2]_{atm}$ is 840 ppm at the triple point in the NaCl-free system (Fig. 3). The upper $[CO_2]_{atm}$ limit for the EECO is unconstrained from the nahcolite proxy, but fluid-inclusion homogenization temperatures of 28 °C suggest that $[CO_2]_{atm}$ in the EECO could have been 1260 ppm.

Microbially Influenced pCO_2 and Contemporaneous Nahcolite and Trona

High $[CO_2]$ needed to form nahcolite may also have been produced in lake waters and bottom sediments of the Piceance Creek Basin by organic processes. Positive $\delta^{13}C$ values measured from nahcolite in the Piceance Creek Basin (+0.09‰ to +20‰) suggest ^{13}C enrichment of CO_2 by methanogenic bacterial processes, or photosynthesis, which removes carbon enriched in ^{12}C, leaving lake waters with high $\delta^{13}C$, especially those with long residence times (Reitsema, 1980; Pitman, 1996; Mees et al., 1998). However, ^{13}C enrichment may also occur inorganically during evaporative concentration of lake waters and degassing of CO_2 concurrent with evaporation (Smith et al., 1987; Mees et al., 1998). Positive $\delta^{13}C$ values from bedded nahcolite in the Piceance Creek Basin do not resolve whether or not the high $[CO_2]$ needed to form nahcolite was generated by organic processes. Large-scale segregation of sodium carbonate minerals (only bedded trona in the Bridger Basin of Wyoming and bedded nahcolite exclusively in the Piceance Creek Basin), on the other hand, is not consistent with local biological controls of CO_2-enriched microenvironments, which change dramatically in time and space. Organic-rich "oil shale" occurs in the Bridger and Piceance Creek Basins, which indicates that biologically productive lakes existed in both basins, and which further argues against pervasive biological control of the $[CO_2]$ levels at which nahcolite or trona precipitated.

The reasons for contemporaneous precipitation of trona in the Bridger Basin and nahcolite in the Piceance Creek Basin are not fully known, but explanations may involve differences in brine chemistry and temperature. Trona, not nahcolite, forms at high activities of Na^+ (a_{Na^+}) and high pH:

$$2NaHCO_3\,(\text{nahcolite}) + 2H_2O + Na^+ \rightleftharpoons NaHCO_3 \cdot Na_2CO_3 \cdot 2H_2O\,(\text{trona}) + H^+. \quad (4)$$

The stability of trona and nahcolite is also controlled by temperature, with nahcolite favored at lower temperatures and trona at higher temperatures, all at the same elevated $[CO_2]_{atm}$ (Fig. 3). Nahcolite could then have precipitated in the Piceance Creek Basin because of its higher elevation while trona formed in the hotter, lower-elevation Bridger Basin. Arguments against this scenario, however, are the north-to-south regional paleodrainage patterns and probable lake spillover from overfilled northern lakes of the Greater Green River Basin to the southern Piceance Creek Basin at ca. 49 Ma (Smith and Carroll, 2015).

CONCLUSIONS

The range of 680–1260 ppm $[CO_2]_{atm}$ for the EECO is well below previously reported values from the nahcolite proxy (1125 ppm to 2985 ppm) (Lowenstein and Demicco, 2006) and is in better agreement with new estimates from paleosols and leaf stomata, as well as the GEOCARB III (ftp://ftp.ncdc.noaa.gov/pub/data/paleo/climate_forcing/trace_gases/phanerozoic_co2.txt) long-term carbon cycle model (Berner and Kothavala, 2001) (Fig. 1). High deep-sea temperatures of ~12 °C for the EECO (Zachos et al., 2008) and estimated global surface air temperatures of ~28 °C at 50 Ma

(Hansen et al., 2013) coincide with nahcolite deposition in the Green River Formation, which suggests a causal link between global warmth and elevated $[CO_2]_{atm}$ during the warmest period of the Cenozoic (Fig. 1). The new, significantly lower estimates of $[CO_2]_{atm}$ in the EECO imply an equilibrium sensitivity of just over twice the ~3 °C per $[CO_2]_{atm}$ doubling that is assumed (Hansen et al., 2008), suggesting that Earth's climate may be more sensitive to a doubling of $[CO_2]_{atm}$ than is currently thought.

ACKNOWLEDGMENTS

We thank D. Royer for providing ancient $[CO_2]_{atm}$ data, P. Wilf and P. Barrett for constructive discussions and development of this manuscript, and E. Thomas and three anonymous reviewers for their careful reviews. A Geological Society of America Research Grant and the Center for Oil Shale Technology and Research (COSTAR) at Colorado School of Mines supported this work.

REFERENCES CITED

Beerling, D.J., Fox, A., and Anderson, C.W., 2009, Quantitative uncertainty analyses of ancient atmospheric CO_2 estimates from fossil leaves: American Journal of Science, v. 309, p. 775–787, doi:10.2475/09.2009.01.

Berner, R.A., and Kothavala, Z., 2001, GEOCARBIII: A revised model of atmospheric CO_2 over Phanerozoic time: American Journal of Science, v. 301, p. 182–204, doi:10.2475/ajs.301.2.182.

Breecker, D.O., Sharp, Z.D., and McFadden, L.D., 2010, Atmospheric CO_2 concentrations during ancient greenhouse climates were similar to those predicted for A.D. 2100: Proceedings of the National Academy of Sciences of the United States of America, v. 107, p. 576–580, doi:10.1073/pnas.0902323106.

Cerling, T.E., 1992, Use of carbon isotopes in paleosols as an indicator of the $P(CO_2)$ of the paleoatmosphere: Global Biogeochemical Cycles, v. 6, p. 307–314, doi:10.1029/92GB01102.

Cotton, J.M., and Sheldon, N.D., 2012, New constraints on using paleosols to reconstruct atmospheric pCO_2: Geological Society of America Bulletin, v. 124, p. 1411–1423, doi:10.1130/B30607.1.

Dyni, J.R., 1996, Sodium carbonate resources of the Green River Formation in Utah, Colorado, and Wyoming: U.S. Geological Survey Open-File Report 96-729, 42 p.

Ekart, D.D., Cerling, T.E., Montañez, I.P., and Tabor, N.J., 1999, A 400 million year carbon isotope record of pedogenic carbonate: Implications for paleoatmospheric carbon dioxide: American Journal of Science, v. 299, p. 805–827, doi:10.2475/ajs.299.10.805.

Eugster, H.P., 1966, Sodium carbonate-bicarbonate minerals as indicators of pCO_2: Journal of Geophysical Research, v. 71, p. 3369–3377, doi:10.1029/JZ071i014p03369.

Fletcher, B.J., Brentnall, S.J., Anderson, C.W., Berner, R.A., and Beerling, D.J., 2008, Atmospheric carbon dioxide linked with Mesozoic and early Cenozoic climate change: Nature Geoscience, v. 1, p. 43–48, doi:10.1038/ngeo.2007.29.

Franks, P.J., Royer, D.L., Beerling, D.J., Van de Water, P.K., Cantrill, D.J., Barbour, M.M., and Berry, J.A., 2014, New constraints on atmospheric CO_2 concentration for the Phanerozoic: Geophysical Research Letters, v. 41, p. 4685–4694, doi:10.1002/2014GL060457.

Greenwood, D.R., Scarr, M.J., and Christophel, D.C., 2003, Leaf stomatal frequency in the Australian tropical rainforest tree *Neolitsea dealbata* (Lauraceae) as a proxy measure of atmospheric pCO_2: Palaeogeography, Palaeoclimatology, Palaeoecology, v. 196, p. 375–393, doi:10.1016/S0031-0182(03)00465-6.

Hansen, J., Sato, M., Kharecha, P., Beerling, D., Masson-Delmotee, V., Pagani, M., Raymo, M., Royer, D.L., and Zachos, J.C., 2008, Target atmospheric CO_2: Where should humanity aim?: Open Atmospheric Science Journal, v. 2, p. 217–231, doi:10.2174/1874282300802010217.

Hansen, J., Sato, M., Russell, G., and Kharecha, P., 2013, Climate sensitivity, sea level and atmospheric carbon dioxide: Philosophical Transactions of the Royal Society A, v. 371, p. 20120294, doi:10.1098/rsta.2012.0294.

Hyland, E.G., and Sheldon, N.D., 2013, Coupled CO_2-climate response during the Early Eocene Climatic Optimum: Palaeogeography, Palaeoclimatology, Palaeoecology, v. 369, p. 125–135, doi:10.1016/j.palaeo.2012.10.011.

Hyland, E., Sheldon, N.D., and Fan, M., 2013, Terrestrial paleoenvironmental reconstructions indicate transient peak warming during the early Eocene climatic optimum: Geological Society of America Bulletin, v. 125, p. 1338–1348, doi:10.1130/B30761.1.

Johnson, R.C., 1981, Stratigraphic evidence for a deep Eocene Lake Uinta, Piceance Creek Basin, Colorado: Geology, v. 9, p. 55–62, doi:10.1130/0091-7613(1981)9<55:SEFADE>2.0.CO;2.

LaClair, D., and Lowenstein, T.K., 2010, Using microthermometry, laser Raman spectroscopy and evaporites to reconstruct the paleoclimate of the Eocene Green River Formation, Colorado, USA, *in* Proceedings of the 10th Biennial Pan-American Current Research on Fluid Inclusions, University of Nevada Las Vegas, Las Vegas, Nevada, 7–1 June 2010, p. 51–52.

Lowenstein, T.K., and Demicco, R.V., 2006, Elevated Eocene atmospheric CO_2 and its subsequent decline: Science, v. 313, p. 1928, doi:10.1126/science.1129555.

Lowenstein, T.K., and Hardie, L.A., 1985, Criteria for the recognition of salt-pan evaporites: Sedimentology, v. 32, p. 627–644, doi:10.1111/j.1365-3091.1985.tb00478.x.

McElwain, J.C., 1998, Do fossil plants signal palaeoatmospheric CO_2 concentration in the geological past?: Philosophical Transactions of the Royal Society of London. Series B, Biological Sciences, v. 353, p. 83–96, doi:10.1098/rstb.1998.0193.

Mees, F.M., Reyes, E., and Keppens, E., 1998, Stable isotope chemistry of gaylussite and nahcolite from deposits of the crater lake at Malha, northern Sudan: Chemical Geology, v. 146, p. 87–98, doi:10.1016/S0009-2541(98)00006-0.

Neev, D., and Emery, K.O., 1967, The Dead Sea: Depositional Processes and Environments of Evaporites: Israel Geologic Survey Bulletin 41, 147 p.

Pearson, P.N., and Palmer, M.R., 2000, Atmospheric carbon dioxide concentrations over the past 60 million years: Nature, v. 406, p. 695–699, doi:10.1038/35021000.

Pitman, J.K., 1996, Origin of primary and diagenetic carbonates in the lacustrine Green River Formation (Eocene), Colorado and Utah: U.S. Geological Survey Bulletin 2157, 17 p.

Reitsema, R.H., 1980, Dolomite and nahcolite formation in organic rich sediments: Isotopically heavy carbonates: Geochimica et Cosmochimica Acta, v. 44, p. 2045–2049, doi:10.1016/0016-7037(80)90202-1.

Retallack, G.J., 2001, A 300-million-year record of atmospheric carbon dioxide from fossil plant cuticles: Nature, v. 411, p. 287–290, doi:10.1038/35077041.

Royer, D.L., 2003, Estimating latest Cretaceous and Tertiary atmospheric CO_2 from stomatal indices, *in* Wing, S.L., et al., eds., Causes and Consequences of Globally Warm Climates in the Early Paleogene: Geological Society of America Special Paper 369, p. 79–93, doi:10.1130/0-8137-2369-8.79.

Royer, D.L., 2014, Atmospheric CO_2 and O_2 during the Phanerozoic: Tools, patterns, and impacts, *in* Holland, H.D., and Turekian, K.K., eds., Treatise on Geochemistry (second edition): New York, Oxford University Press, p. 251–267, doi:10.1016/B978-0-08-095975-7.01311-5.

Royer, D.L., Wing, S.L., Beerling, D.J., Jolley, D.W., Koch, P.L., Hickey, L.J., and Berner, R.A., 2001, Paleobotanical evidence for near present-day levels of atmospheric CO_2 during part of the Tertiary: Science, v. 292, p. 2310–2313, doi:10.1126/science.292.5525.2310.

Royer, D.L., Pagani, M., and Beerling, D.J., 2012, Geobiological constraints on Earth system sensitivity to CO_2 during the Cretaceous and Cenozoic: Geobiology, v. 10, p. 298–310, doi:10.1111/j.1472-4669.2012.00320.x.

Sinha, A., and Stott, L.D., 1994, New atmospheric pCO_2 estimates from paleosols during the late Paleocene/early Eocene global warming interval: Global and Planetary Change, v. 9, p. 297–307, doi:10.1016/0921-8181(94)00010-7.

Smith, G.I., Friedman, I., and McLaughlin, R.J., 1987, Studies of Quaternary saline lakes: III. Mineral, chemical, and isotopic evidence of salt solution and crystallization processes in Owens Lake, California, 1969–1971: Geochimica et Cosmochimica Acta, v. 51, p. 811–827, doi:10.1016/0016-7037(87)90095-0.

Smith, M.E., and Carroll, A.R., 2015, Introduction to the Green River Formation, *in* Smith, M.E., and Carroll, A.R., eds., Stratigraphy and Paleolimnology of the Green River Formation, Western USA: Syntheses in Limnology, v. 1, p. 1–12, doi:10.1007/978-94-017-9906-5_1.

Smith, R.Y., Greenwood, D.R., and Basinger, J.F., 2010, Estimating paleoatmospheric pCO_2 during the Early Eocene Climatic Optimum from stomatal frequency of *Ginkgo*, Okanagan Highlands, British Columbia, Canada: Palaeogeography, Palaeoclimatology, Palaeoecology, v. 293, p. 120–131, doi:10.1016/j.palaeo.2010.05.006.

Wilf, P., 2000, Late Paleocene–early Eocene climate changes in southwestern Wyoming: Geological Society of America Bulletin, v. 112, p. 292–307, doi:10.1130/0016-7606(2000)112<292:LPECCI>2.0.CO;2.

Yapp, C.J., 2004, $Fe(CO_3)OH$ in goethite from a mid-latitude North American Oxisol: Estimate of atmospheric CO_2 concentration in the Early Eocene "climatic optimum": Geochimica et Cosmochimica Acta, v. 68, p. 935–947, doi:10.1016/j.gca.2003.09.002.

Zachos, J.C., Dickens, G.R., and Zeebe, R.E., 2008, An early Cenozoic perspective on greenhouse warming and carbon-cycle dynamics: Nature, v. 451, p. 279–283, doi:10.1038/nature06588.

Zhang, Y.G., Pagani, M., Liu, Z., Bohaty, S.M., and DeConto, R., 2013, A 40-million-year history of atmospheric CO_2: Philosophical Transactions of the Royal Society A, v. 371, p. 1–20, doi:10.1098/rsta.2013.0096.

Manuscript received 11 April 2015
Revised manuscript received 9 October 2015
Manuscript accepted 12 October 2015

Printed in USA